Amino Acids (2011) 41:415–425
DOI 10.1007/s00726-010-0733-x

ORIGINAL ARTICLE

Influence of RET/PTC1 and RET/PTC3 oncoproteins in radiation-induced papillary thyroid carcinomas on amounts of cytoskeletal protein species

Evelyn Zeindl-Eberhart · Sibylle Liebmann · Peter Roman Jungblut · Jens Mattow · Monika Schmid · Rosi Kerler · Hartmut Manfred Rabes

Received: 31 March 2010 / Accepted: 26 August 2010 / Published online: 14 September 2010

Abstract Radiation-induced human papillary thyroid carcinomas (PTCs) show a high prevalence of fusions of the *RET* proto-oncogene to heterologous genes *H4* (*RET/PTC1*) and *ELE1* (*RET/PTC3*), respectively. In contrast to the normal membrane-bound RET protein, aberrant RET fusion proteins are constitutively active oncogenic cytosolic proteins that can lead to malignant transformation of thyroid epithelia. To detect specific tumor-associated protein changes that reflect the effect of RET/PTC fusion proteins, we analyzed normal thyroid tissues, thyroid tumors of the RET/PTC1 and RET/PTC3 type and their respective lymph node metastases by a combination of high-resolution two-dimensional electrophoresis and matrix-assisted laser desorption/ionization-mass spectrometry. PTCs without RET rearrangements served as controls. Several cytoskeletal protein species showed quantitative changes in tumors and lymph node metastases harboring RET/PTC1 or RET/PTC3. We observed prominent C-terminal actin fragments assumedly generated by protease cleavages induced due to enhanced amounts of the active actin-binding protein cofilin-1. In addition, three truncated vimentin species, one of which was proven to be headless, were shown to be highly abundant in tumors and metastases of both RET/PTC types. The observed protein changes are closely connected with the constitutive activation of RET-rearranged oncoproteins and reflect the importance to elucidate disease-related typical signatures on the protein species level.

Keywords Papillary thyroid carcinoma · PTC1 · PTC3 · Proteome analysis · Protein species

Abbreviations

PTC	Papillary thyroid carcinoma
RET	Rearranged during transfection proto-oncogene
RET/PTC1	*RET* gene rearrangement with *H4* gene
PTC1	Papillary thyroid carcinoma with *RET/PTC1*
RET/PTC3	*RET* gene rearrangement with *ELE1* gene
PTC3	Papillary thyroid carcinoma with *RET/PTC3*
PTC0	PTC without RET rearrangement
TK	Tyrosine kinase
TAPs	Tumor-associated protein changes
MAPs	Metastasis-associated protein changes
N	Normal thyroid tissue
T	PTC1-, PTC3-, PTC0-tumor
M	Lymph node metastasis
IF	Intermediate filaments
MAPK	Mitogen-activated protein kinase

Introduction

The development of papillary thyroid carcinomas (PTCs) has been reported in children exposed to radioactive fallout

Electronic supplementary material The online version of this article (doi:10.1007/s00726-010-0733-x) contains supplementary material, which is available to authorized users.

E. Zeindl-Eberhart (✉) · S. Liebmann · R. Kerler · H. M. Rabes
Institute of Pathology,
Ludwig-Maximilians-University of Munich,
Thalkirchner Strasse 36, 80337 Munich, Germany
e-mail: Evelyn.ZeindlEberhart@med.uni-muenchen.de

P. R. Jungblut · J. Mattow · M. Schmid
Max-Planck Institute for Infection Biology,
10117 Berlin, Germany

after the reactor accident in Chernobyl, particularly in highly contaminated regions of Belarus. Molecular analysis of post-Chernobyl PTC revealed, at short intervals after the accident, a very high prevalence of *RET* proto-oncogene rearrangements (Klugbauer et al. 1995; Nikiforov et al. 1997; Rabes et al. 2000). These rearrangements are characterized by fusion of the *RET* tyrosine kinase (TK)-encoding domain and 5′ parts of various other genes that lead to the generation of different chimeric *RET/PTC* oncogenes (for review, see Rabes 2001). The predominant variants *RET/PTC1* and *RET/PTC3* involve the genes *H4* (Greco et al. 1999; Pierotti et al. 1992) and *ELE1* (Santoro et al. 1994; Bongarzone et al. 1994), respectively. *RET/PTC3* rearrangements prevail during the early, *RET/PTC1* at later intervals after irradiation (Rabes et al. 2000).

The proto-*RET* encodes a membrane-associated receptor TK that is produced at specific developmental stages in cells derived from the neural crest including sympathic ganglia, adrenal medulla and thyroid C cells, and cells of the excretory system of the developing kidney. RET is the receptor for the glial cell-derived neurotrophic factor (GDNF) family. It is activated by its homodimerization and autophosphorylation at specific tyrosine residues. RET triggers several intracellular signaling cascades, which regulate, dependent on the cell type, survival, differentiation, proliferation, migration, chemotaxis, branching morphogenesis, neurite outgrowth and synaptic plasticity (Airaksinen et al. 1999; Sariola and Saarma 2003).

RET/PTC1 and *RET/PTC3* are formed when *RET* undergoes a translocation fusing its 3′ *TK* domain to a 5′ part of another gene that replaces the *RET* promoter, the extracellular ligand binding domain and the membrane anchoring domain. The genes that are predominantly fused to *RET*, *H4* and *ELE1* are ubiquitously expressed, including thyroid follicular epithelium. It has been discovered that H4 is involved in the induction of apoptosis in thyroid follicular epithelial cells (Celetti et al. 2004). ELE1 (ARA70) functions as a transcriptional coactivator of androgen receptor (Yeh and Chang 1996). Various functional consequences of *RET* rearrangements have been discussed with regard to oncogenic activation: (a) transcriptional activation of *RET* due to the novel 5′ promoter of the chimeric genes, (b) translocation of RET/PTC proteins into cytoplasm due to the deletion of the transmembrane anchoring sequence, and (c) constitutive upregulation of RET signaling due to the dimerization potential of 5′ fused genes and tyrosine autophosphorylation of RET/PTC proteins. As a consequence of aberrant RET upregulation, the normal cell metabolism is deranged. Protein alterations in PTC might reflect this dysregulation due to *RET* gene rearrangements.

Recent studies disclosed that the type of genetic alterations is decisive for the tumor phenotype: *RET/PTC1* rearrangements were found mainly in papillary and follicular variants, while in tumors with *RET/PTC3* rearrangements the solid variant of PTC was most frequently observed (Rabes et al. 2000; Thomas et al. 1999). The presence and activity of RET/PTC mutant protein appears sufficient to induce typical morphological changes that are characteristic for PTC (Barone et al. 2001; Fischer et al. 1998; Mai et al. 2001; Fusco et al. 2002), but might be different in PTC without RET/PTC rearrangement. To explore if these differences are reflected by a specific pattern of quantitative and/or qualitative protein changes, we performed comparative proteome analyses of normal thyroid tissues, thyroid tumor tissues and lymph node metastases as a function of the type of RET rearrangement, PTC1 or PTC3, and in PTC without RET rearrangement. Soluble and insoluble protein fractions were extracted and separated by high-resolution two-dimensional electrophoresis (2-DE). Protein spots showing significant changes in spot intensity, which are characteristic for PTC1 and/or PTC3 tumors, were identified by matrix-assisted laser desorption/ionization-mass spectrometry (MALDI-MS). Sixty-two tumor-associated protein changes (TAPs) were identified and could be assigned to different protein families and functions. In this contribution, we focused on TAPs that are related to the cytoskeleton.

Our analysis revealed several cytoskeletal protein species, namely from actin, vimentin and the actin-binding protein cofilin-1, showing marked quantitative changes assumedly due to the constitutive activity of RET/PTC1 or RET/PTC3 fusion proteins in the radiation-induced papillary thyroid tumors investigated. It exemplifies that proteomics provides the possibility to elucidate downstream regulatory effects caused by genetic alterations and demonstrates that the combination of molecular biology and proteomics offers a valuable approach for in-depth analysis of correlations between genomic alterations and phenotype in human thyroid carcinomas.

Materials and methods

Tissue specimen

Normal human thyroid tissues, PTCs and their respective lymph node metastases were studied. In a preceding molecular analysis, the type of *RET* rearrangement, either *RET/PTC1* or *RET/PTC3* or missing *RET* rearrangement (designated PTC0), has been determined (Rabes et al. 2000). The tumor material was obtained from 17 female patients who had been exposed during childhood (mean age 4.8 ± 4.1 years) to the radioactive fallout after the reactor accident in Chernobyl. The tissue samples have been collected between 1997 and 1998 from these patients (mean age at surgery 16.7 ± 4.0 years; tumor latency

12.1 ± 0.43 years) with informed consent. They underwent thyroidectomy at the Department of Surgery, Medical High School of Minsk, Belarus. At surgery, small tissue samples were frozen in dry ice and subsequently stored at −80°C until further processing.

We compared sets of samples from each individual patient comprising normal human thyroid tissue, primary PTC and, if available, lymph node metastases. For PTC1, material was obtained from six normal thyroid tissues, six PTCs and three lymph node metastases. PTC3 samples were analyzed from six normal thyroid tissues, five tumors and five lymph node metastases. In case of PTC0, five normal thyroid tissues, five thyroid carcinomas and three lymph node metastases were studied. All samples were histologically verified (Rabes et al. 2000).

Preparation of protein samples

Soluble and insoluble proteins were extracted from tissues samples according to Klose (1999).

Two-dimensional gel electrophoresis

Proteins were separated by high-resolution 2-DE (Klose and Kobalz 1995) using the Iso-Dalt-equipment (Hoefer Scientific Instruments, San Francisco, CA, USA). IEF (first dimension) was performed in rod gels (inner diameter 1.5 mm, length 18 cm), containing 4% carrier ampholytes (4 parts Servalyte, pH 5–7, Serva, Heidelberg, Germany; 1 part Pharmalyte, pH 3–10 and 1 part Ampholine, pH 3.5–9.5, both Amersham Pharmacia Biotech, Uppsala, Sweden), SDS-PAGE (second dimension) was run on gels (16 cm × 16 cm × 1.5 mm) with a 10–16% polyacrylamide gradient (Zeindl-Eberhart and Rabes 1992). 100 µg of protein sample (Lowry protein assay kit, Sigma-Aldrich, Deisenhofen, Germany) was applied for analytical silver-stained 2-DE gels (Jungblut and Seifert 1990). In case of preparative Coomassie Brilliant Blue R-250 (CBB R250; Merck, Darmstadt, Germany)-stained 2-DE gels and immunoblots, 400 µg of protein sample was used.

The soluble and the insoluble protein fractions of each sample ($n = 44$) were analyzed by 2-DE at least twice. Because of the variable amount of albumin, most notably in the soluble fraction (1st run), the applied protein amount was adjusted to approximately similar amounts of different internal standard proteins which were similar in amount in normal thyroid tissues, thyroid carcinomas as well as in lymph node metastases (2nd run).

To elucidate potential protein variations, at first 2-DE gels of normal human thyroid tissues and gels of corresponding PTC1 or PTC3 tumor material were individually compared (as gel pairs). All protein spots that show differences in intensity in the PTCs investigated ($n = 6$ for PTC1; $n = 5$ for PTC3) were defined as putative candidates for TAPs. These were finally verified by cross-comparison of all TAPs in 2-DE gels. Only stringently confirmed differences were accepted as TAPs. Gel comparisons were performed using the image analysis software program TOPSPOT, which is available at http://www.mpiib-berlin.mpg.de/2D-PAGE/. Representative 2-DE gels of the soluble and the insoluble protein fractions of normal thyroid tissues were used as master gels. Spot intensities were normalized against protein spots of the soluble and the insoluble protein fractions, respectively, which did not vary between normal thyroid tissues, thyroid carcinomas or lymph node metastases. In order to evaluate significant TAPs, a Student's t test ($P \leq 0.05$) was performed. To define PTC1- and/or PTC3-specific TAPs, all PTC1 and PTC3 TAPs were verified by means of 2-DE gels of PTC0 material and their corresponding normal thyroid tissues. Only significant TAPs observed in PTC1 and/or PTC3 gels as compared to normal thyroid tissues, but not in PTC0 tumors were accepted as specific.

In addition, all TAPs observed in PTC1 and/or PTC3 gels were verified by means of the corresponding lymph node metastases. Spots that were significantly changed in intensity compared with their analogous TAPs ($P \leq 0.05$) were defined as metastasis-associated protein changes (MAPs). All PTC1 and/or PTC3 MAPs were compared with 2-DE gels of lymph node metastases from PTC0 patients according to the criteria outlined above.

Protein identification

For protein identification, spots of interest were excised from CBB-stained gels and subjected to in-gel digestion using trypsin, alternatively GluC was used as an endoproteinase (Lamer and Jungblut 2001). The resulting peptides were freed of salt and concentrated using ZipTipC_{18} pipette tips (Millipore, Bedford, USA). Their masses were determined using a time-of-flight mass spectrometer (Voyager Elite; Applied Biosystems, Framingham, USA) with delayed extraction operated in the reflectron mode. The spectra were calibrated using synthetic peptides with known molecular mass as internal markers. Proteins were identified by peptide mass fingerprinting (PMF) using the search algorithms MS-Fit (http://prospector.ucsf.edu/) and/or PeptIdent (http://au.expasy.org/tools/peptident.html). The experimentally derived peptide masses were compared against theoretical peptide mass data of all human/rodent proteins stored in the National Centre for Biotechnology Information (NCBI) and/or SwissProt (SP) database, as described (Lamer and Jungblut 2001; Zeindl-Eberhart et al. 2001). The tolerated mass error was 100 ppm. Partial enzymatic cleavages leaving two cleavage sites, acetylation of N-termini of proteins,

pyroglutamate formation at N-terminal glutamine of peptides, oxidation of methionine and modification of cysteine by acrylamide were considered as possible modifications. The primary identification criterion was a sequence coverage ≥30%.

Immunoblotting

For immunoblotting, the soluble protein fraction of normal thyroid tissue and the corresponding PTC1 tumor was used for the immunodetection of p-cofilin-1, for vimentin the insoluble protein fraction of normal thyroid tissue and the corresponding PTC3 tumor was taken. After 2-DE, gel areas containing spots of interest, namely human cofilin (~25–14 kDa/p*I* ~ 6–8.2) and vimentin (~40–70 kDa/p*I* ~ 4–6), were excised and blotted under semi-dry conditions onto hydrophobic 0.2 µm PVDF (Bio-Rad, Hercules, CA, USA) membranes (2 h at 1 mA/cm^2). 50 mM borate buffer, pH 9.0 containing 20% methanol was used as anode/cathode buffer (Zeindl-Eberhart et al. 1997). The cathode buffer was additionally supplemented with 0.1% SDS (Sigma-Aldrich, München, Germany). The blotted membranes were washed in TBS and blocked for 1 h in PBS/0.1% Tween 20 (PBS/Tween) supplemented with 5% non-fat dry milk powder (Bio-Rad). Afterward, the membranes were incubated for 17 h at 4°C with the first antibody (in PBS/Tween, 5% dry milk), washed three times in PBS/Tween, incubated for 1 h with the HRP-coupled secondary antibody (in PBS/Tween, 5% dry milk) and once again washed three times. For immunodetection of p-cofilin-1 and vimentin, the polyclonal antibodies p-cofilin-1 (Ser3-R; Santa Cruz Biotechnology Inc., Santa Cruz, USA) and vimentin (H-84; Santa Cruz Biotechnology Inc.) as well as the monoclonal anti-vimentin (clone vim 13.2; Sigma-Aldrich) were used at a dilution of 1:1,500. The secondary antibodies (anti-rabbit, anti-mouse, respectively) were used at a dilution of 1:5,000. The signals were intensified using the enhanced chemoluminescence (ECL) detection kit (Amersham Pharmacia Biotech, Uppsala, Sweden). To strip off primary and secondary antibodies, membranes were incubated (30 min at 50°C) in 62.5 mM Tris–HCl buffer (pH 6.7) supplemented with 100 mM 2-mercaptoethanol and 2% SDS (all Sigma). The immunodetection was repeated as described above.

Results

The present study aimed at the identification of specific protein changes induced by RET/PTC1 and/or RET/PTC3 fusion proteins. We analyzed sets of samples from individual patients, comprising normal human thyroid tissue, primary PTC and lymph node metastases of the PTC1 and PTC3 types, by a combination of high-resolution 2-DE and MALDI-MS. PTC without RET rearrangements served as controls for the determination of PTC1 and/or PTC3 specificity.

2-DE patterns of the soluble and insoluble protein fractions of all samples investigated were highly reproducible. Representative 2-DE gels of both protein fractions of PTC are shown in Figs. 1a (soluble proteins) and 2a (insoluble proteins). Sixty-two quantitative PTC1- and/or PTC3-specific TAPs as well as specific MAPs were detected and could be assigned to different protein families and functions. A number of variant protein spots were identified as proteins involved in metabolism, detoxification, chaperone/stress response, signal transduction, transport, ion channels, as well as proteins responsible for protein synthesis and degradation or as cytoskeletal proteins. In this publication, we describe changes concerning proteins functionally associated with the cytoskeleton and due to their appearance as different protein species.

Seven TAPs were identified in PTC1 and PTC3 tumors. Four MAPs were detected by comparison with their analogous TAPs in PTC1 and PTC3 lymph node metastases. The identified variant spots represent three distinct proteins: actin, cofilin-1 and vimentin. They were shown to give rise to more than one protein spot, i.e. different protein species (Table 1).

Certain regions of the gels in Figs. 1a and 2a were designated as region-1 and region-2. They include several significant TAPs and MAPs. These regions are shown in more detail in Figs. 1b and 2b, respectively. Additional spots identified as TAPs and/or MAPs outside of these regions are also marked by arrows in Figs. 1a and 2a.

Tumor- and metastasis-associated protein changes detected in PTC1 and PTC3 samples

Several characteristic changes in protein abundance were detected in 2-DE gels of the soluble protein fractions of PTC1 and/or PTC3 samples. In region-1 (Fig. 1b), three prominent protein spots (23, 24 and 25) are marked by arrows in 2-DE gels of normal thyroid tissues (N). All these spots showing the same apparent p*I* (5.6) but differing with regard to their Mr (37, 33 and 28 kDa) were identified by PMF as N-terminally truncated actin. In PTC1 and PTC3 tumors (T), the amount of these actin species is markedly elevated. Significantly increased intensities were also registered for spots 24 and 25 in lymph node metastases (M) of PTC1 and for spot 23 in PTC3. In PTC0 material, no significant changes of these spots could be observed. Interestingly, the intensity of the full-length actin (43.0 kDa/p*I* 5.3) did not vary significantly in the investigated tissue material, its position is marked in Fig. 1a.

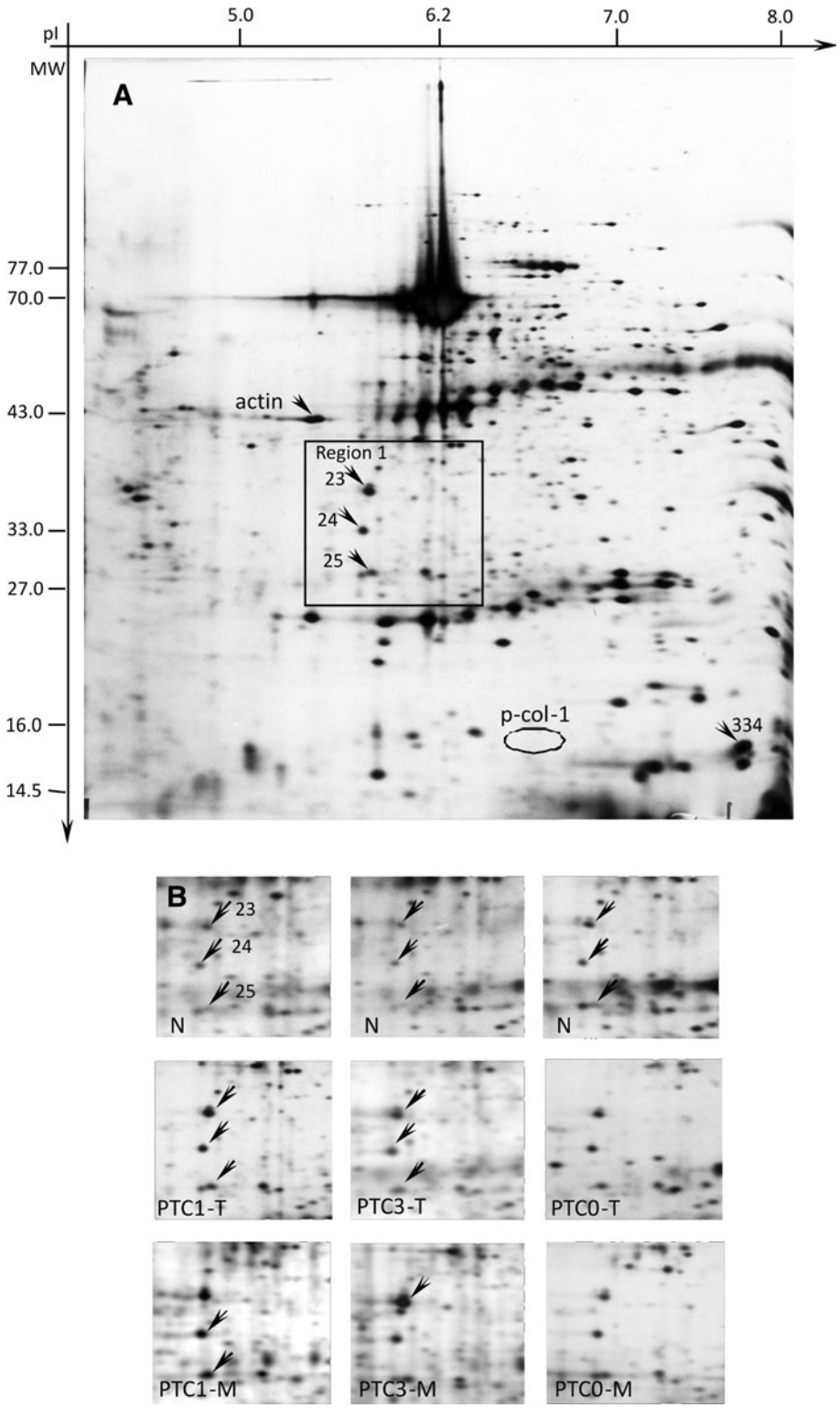

Fig. 1 Different actin species showed tumor-associated intensity changes in PTC1 and PTC3. **a** 2-DE gel of soluble proteins from papillary thyroid carcinoma. 100 µg of soluble proteins was separated in the first dimension by isoelectric focusing using 4% carrier ampholytes (pH 3–10). Separation in the second dimension was performed using an acrylamide gradient (10–16%) followed by silver staining. Mr axis was calibrated by standard proteins (Serva). *Framed area* designated as region-1 shows tumor-associated protein changes (TAPs) (*arrows*). These were identified by PMF as actin species. The quantitative changes are shown in more detail in **b**. The variant spot 334 was identified as the activated actin-binding protein cofilin-1 (*arrow*), the position of phosphorylated cofilin-1 (p-col-1) is *encircled* and shown in supplement Figure 2a. The identity of all TAPs is summarized in Table 1. **b** In the soluble protein fractions of normal thyroid tissues (N), papillary thyroid carcinomas of the PTC1 and PTC3 type (T) and in lymph node metastases (M), three different spots (23, 24 and 25) representing actin were detected (region-1). PTC0 samples served as a control (N, T, M) for the determination of PTC1 and/or PTC3 specificity. *Arrows* in PTC-T and -M areas indicate identified spots showing significant changes ($P \leq 0.05$) in protein abundance between normal and PTC or between tumors and lymph node metastases

Spot 334 (Fig. 1a; supplement Figure 1a), identified as cofilin-1 (16.0 kDa/p*I* 8.0), showed a significantly increased intensity in PTC1 tumors. Cofilin-1 was also detected in the insoluble protein fraction (spot 534) (Fig. 2a; supplement Figure 1b). Here, it displayed significantly elevated amounts in PTC1 tumors as well as in PTC3 tumors and lymph node metastases (Table 1). Spots 334 and 534 were not detectable by an antibody directed against p-cofilin-1 (recognizing

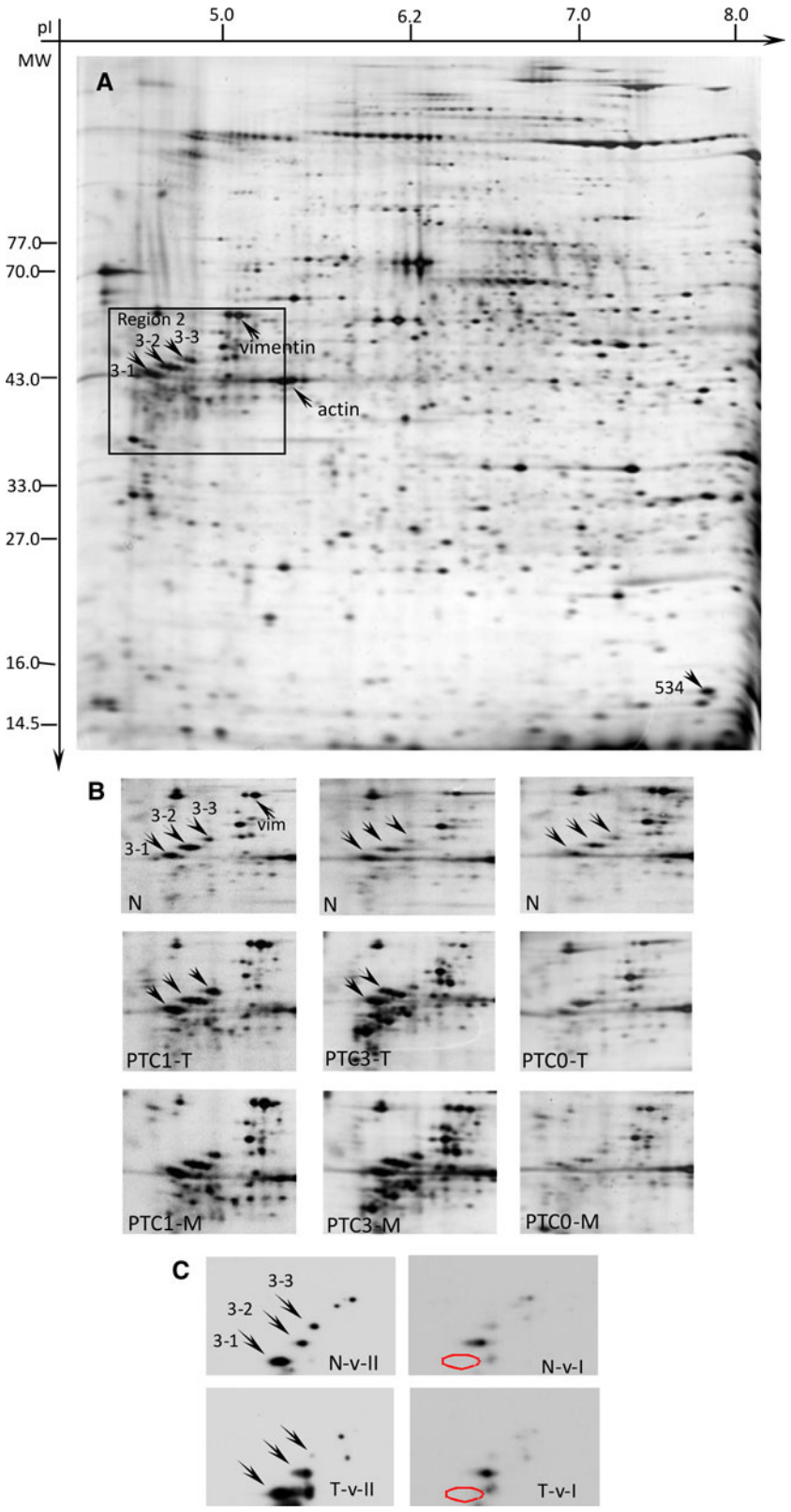

Fig. 2 Different vimentin species were found in PTC1 and PTC3 as tumor-associated intensity changes. **a** Two-dimensional gel of insoluble proteins from papillary thyroid carcinoma. 100 µg of soluble proteins was separated by high-resolution 2-DE, the resulting gel was subjected to silver staining. *Framed area* designated as region-2 shows protein spots (*arrows*) identified by PMF as vimentin (spots 3-1, 3-2 and 3-3). The quantitative changes are shown in more detail in **b**. The protein spot 534 identified as cofilin-1 is marked by an *arrow* and listed in Table 1. **b** In the insoluble protein fractions of papillary thyroid carcinomas of the PTC1 and PTC3 type (T), three variant spots (spots 3-1, 3-2, and 3-3) identified as vimentin were detected (*arrows*). PTC0 samples served as a control (N, T, M) for the determination of PTC1 and/or PTC3 specificity. No significantly altered protein amounts were found in the comparison between PTC and lymph node metastases for the above-mentioned variants. **c** Immunodetection of headless vimentin. Spot 3-1 was detected by the antibody v-II, directed against a C-terminal region of vimentin (clone vim 13.2, Sigma), but was not detected by the antibody v-I, directed against the head region of vimentin (H-84, Santa Cruz) (*N* normal thyroid tissue, *T* PTC3 tumor tissue)

phosphorylated serine 3) indicating that these spots represent dephosphorylated cofilin-1. The phosphorylated variant of cofilin-1 was proven at 16.0 kDa/p*I* 6.4 by immunoblotting, but was not assignable as TAP due to no significant changes in the tumor samples investigated. Its position is marked in Fig. 1a (and depicted in supplement Figure 2).

Table 1 PTC1 and PTC3 tumor-associated protein changes detected in 2-DE gels determined by PMF-MALDI-MS and identified as proteins associated with the cytoskeleton

2-DE		Spot identification (MS Sc.%)	SwissProt/NCBI*				Papillary thyroid carcinoma					
Spot no.	kDa/p*I* observed		AA total	kDa/p*I* calculated	Acc. no.	Identified protein	PTC1		PTC3		PTC0	
							TAP (*P*)	MAP (*P*)	TAP (*P*)	MAP (*P*)	TAP (*P*	MAP (*P*)
25	28/5.6	34%	232	25.8/5.7	A29861*	Actin	↑ (0.006)	↑↑ (0.004)	↑ (0.006)	+	+	+
24	33/5.6	32%	375	42/5.3	P60709	Actin	↑ (0.004)	↑↑ (0.02)	↑ (0.04)	+	+	+
23	37/5.7	30%	375	42/5.3	P60709	Actin	↑ (0.002)	+	↑ (0.002)	↑↑ (0.05)	+	+
Actin	43/5.3	Gel comparison	375	42/5.3	P60709	Actin beta (nt)	+	+	+	+	+	+
334	16.0/8.0	62%	116	18.5/8.2	P23528	Cofilin-1	↑ (0.007)	+	+	+	+	+
p-col-1	16.0/6.4	Antibody	116	18.5/8.2	P23528	p-cofilin-1	+	+	+	+	+	+
3-1	44/4.4	58%	466	53.7/5.0	P08670	Vimentin	↑ (0.001)	+	↑ (0.01)	+	+	+
3-2	47/4.6	57%	466	53.7/5.0	P08670	Vimentin	↑ (0.0004)	+	↑ (0.03)	+	+	+
3-3	49/4.8	45%	466	53.7/5.0	P08670	Vimentin	↑ (0.002)	+	+	+	+	+
Vim.	55.0/5.1	Antibody	466	53.7/5.0	P08670	Vimentin (nt)	+	+	+	+	+	+
534	16.0/8.0	62%	116	18.5/8.2	P23528	Cofilin-1	↑ (0.002)	+	↑ (0.0002)	↑↑ (0.02)	+	+

The identified protein spots originated from CBB-stained 2-DE gels of either normal thyroid tissues or from PTC1 or PTC3 tumor tissues. Spots 25, 24, 23 and 334 were detected in the soluble protein fraction, spots: 3-1, 3-2, 3-3, and 534 in the insoluble protein fraction. For the evaluation of MS data, the database SwissProt or *NCBI was used. For comparison, the non-truncated forms of actin (nt) and vimentin (nt) and the phosphorylated form of cofilin-1 were added (actin was identified by gel comparison; vimentin (nt) and p-cofilin were identified by immunoblotting)

Sc.% sequence coverage, *AA* amino acids, *Acc. no.* accession no., *TAP* tumor-associated protein changes (quantitative protein changes significantly altered in the comparison between normal and PTC), *MAP* metastases-associated protein changes (quantitative protein changes significantly altered in the comparison between PTC and lymph node metastases), *(nt)* non-truncated protein, *p-col-1* phosphorylated form of-cofilin-1

Degree of protein amount: ↑, increased as TAP compared with control; ↑↑, increased as MAP compared with tumor tissue

P, significant protein changes as evaluated by Student's *t* test, $P \leq 0.05$; +, present, not significantly changed

In region-2 (Fig. 2b), three different spots (3-1, 3-2 and 3-3) of different Mr and p*I* (44, 47 and 49 kDa/p*I* 4.4, 4.6 and 4.8) were identified as vimentin, member of the intermediate filament (IF) family. All these spots were defined as TAPs because of their significantly elevated intensities in PTC1 and PTC3 tumors as compared to normal thyroid tissues. Such increased spot intensities were not observed in PTC0 tumors and lymph node metastases. These vimentin species were identified as different N-terminally truncated vimentin by PMF. For spot 3-1 (44 kDa/p*I* 4.4), the lack of the N-terminal head domain was confirmed by immunoblotting (Fig. 2c). An additional spot was identified as vimentin by immunoblotting. Due to its apparent mass and p*I* (55 kDa/p*I* 5.1) in 2-DE gels, it is reasonable to assume that it represents a full-length variant of vimentin. Interestingly, the intensity of this spot did not vary significantly in the tumors investigated. For comparison, its position is marked in Fig. 2a and b. The relative intensities of the different vimentin species detected as TAPs in PTC1 and PTC3 samples, PTC0 served as control, are graphically depicted in Fig. 3. Immunoblotting and the application of specific antibodies directed against the N- or C-terminal region of vimentin, respectively, led to the detection of additional vimentin species of different Mr and p*I* (40–44 kDa/p*I* 4.3–4.4). However, these species were not significantly changed in intensity and could not be defined as TAPs (supplement Figure 3).

Discussion

PTC1 and PTC3 tumors are characterized by H4/RET and ELE1/RET fusion proteins, respectively. In contrast to membrane-bound RET protein, RET fusion proteins have been described to be oncogenic cytosolic proteins that may lead to malignant transformation of the thyroid epithelial cells. The identified TAPs reflect the effects of these RET/PTC fusion proteins.

In this study, we focused on TAPs concerning proteins whose function is associated with the cytoskeleton. Seven variant 2-DE spots were identified as cytoskeletal proteins, or proteins related to cytoskeletal functions. They could be assigned to three different proteins, namely actin, vimentin and cofilin-1. Most of the detected protein changes were observed in both types of tumor, indicating that they showed no exclusive PTC1 or PTC3 specificity.

The untruncated actin protein was present in 2-DE gels at 43 kDa in comparable amounts in normal thyroid

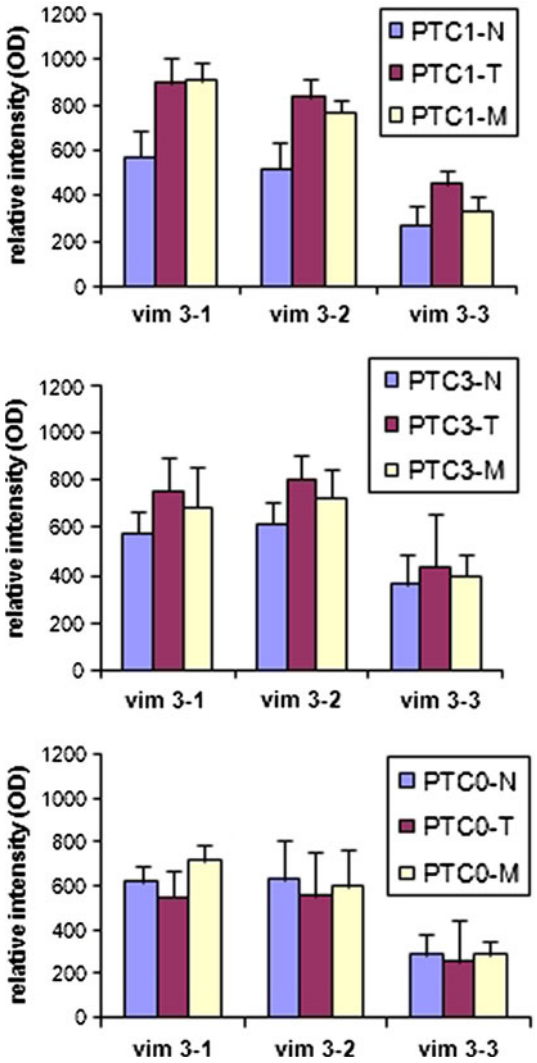

Fig. 3 Quantitation of vimentin species detected as tumor-associated intensity changes in PTC1 and PTC3. Relative intensity (mean ± SD) of different vimentin species (spots 3-1, 3-2 and 3-3) in normal thyroid tissues (PTC-N), papillary thyroid carcinomas (PTC-T) and lymph node metastases (PTC-M) of the PTC1 and PTC3 type and in PTC0 controls. PTC1-N ($n = 6$), PTC1-T ($n = 6$), PTC1-M ($n = 3$), PTC3-N ($n = 6$), PTC3-T ($n = 5$), PTC3-M ($n = 5$), PTC0-N ($n = 5$), PTC0-T ($n = 5$), PTC0-M ($n = 3$)

tissues, thyroid tumors and lymph node metastases. In the soluble protein fractions, we observed several additional protein spots representing actin. These were proven as C-terminal fragments by PMF and showed markedly elevated intensities in PTC1 and PTC3 tumors as well as in lymph node metastases. In PTC0 samples, these actin species were also detectable, but did not display significant changes in tumors and metastases.

The increased amount of some actin species in PTC1 and PTC3 tumors might indicate an enhanced reorganization of the actin cytoskeleton and might be an indirect proof for these activities. Elevated intensities of two spots, identified as the activated dephosphorylated actin-binding protein cofilin-1, a key factor for actin filament remodeling and enhancing actin dynamics (Carlier et al. 1999), found in PTC1 and PTC3 tumors, are in favor for this hypothesis.

Fragmentation of actin may induce actin species and occur due to subtilisin or tryptic cleavage leading to the formation of C-terminal fragments of 37 kDa (Kiessling et al. 1995; Khaitlina and Strzelecka-Golaszewska 2002; Muhlrad et al. 2004) and 34 kDa (Muhlrad et al. 2004), respectively, and correspond to the spots 23 and 24 observed in this investigation. Actin fragmentation might also be induced due to increased levels of activated cofilin-1. Binding to F-actin, it affects conformational changes of the actin filament leading to exposure of subtilisin and trypsin cleavage sites. Protease cleavage initiates a partial disruption of the longitudinal contact between filaments, but not a structural destruction (Muhlrad et al. 2004). Due to preparation of tissue samples for separation of proteins by 2-DE, these actin fragments became visible. However, verification of the exact subtilisin cleavage sites by PMF did not succeed.

The same actin species have also been found in 2-DE gels of some human mammary and hepatocellular carcinomas (unpublished results), though with much lower amounts as compared to PTC1 and PTC3. This suggests that these actin species might be connected to a general reorganization of the actin cytoskeleton in tumor cells. Actin fragments of 15 and 31 kDa were observed in apoptotic cells of certain tumor cell lines as a result of caspase-3-mediated cleavages (Mashima et al. 1999; Brockstedt et al. 1998). These typical apoptotic actin fragments were not detected in our 2-DE gels and are in line with the immunohistochemical proof that apoptosis is a rare event in PTC1 and PTC3 (Basolo et al. 1997).

The full-length vimentin protein was present in 2-DE gels of the insoluble protein fractions at 55 kDa in comparable amounts in normal thyroid tissue, thyroid tumors and in lymph node metastases. Three different truncated vimentin species, significantly increased in PTC1 and PTC3 tumors, were identified. They were proven as C-terminal fragments by PMF. Spot 3-1 was confirmed by an N-terminal head domain-specific vimentin antibody as headless (Andreoli and Trevor 1994) vimentin.

N-terminally truncated vimentin has been observed by 2-DE (Lee et al. 2001; Nylund and Leszczynski 2004) and described as a result of a progressive degradation due to cleavage by caspase (Fujita et al. 2003; Morishima 1999; Hashimoto et al. 1998) or by human immunodeficiency virus type 1 protease (HIV-1PR) (Shoeman et al. 2001). However, the occurrence of N-terminally truncated vimentin does not seem to cause an overt perturbation of IF network because parts of it are able to bind to intact vimentin (Andreoli and Trevor 1994).

Recent reports showed that the head region of vimentin is responsible for its DNA-binding properties (Shoeman et al. 1999; Wang et al. 2000). N-terminal fragments liberated from the IF fail to reassemble (Byun et al. 2001) but are capable to enter into the nucleus and to induce alterations of chromatin distribution (Shoeman et al. 2001) and nuclei with prominently invaginated morphology (Sarria et al. 1994). Supposed that the percentage of C-terminal vimentin in PTC1 and PTC3 tumors is proportional to that of liberated N-terminal head vimentin, it is reasonable to assume that these amounts might exert a striking influence on nuclear morphology. An influence on nuclear morphology has been observed in primary human thyroid epithelial cells infected with a RET/PTC1 retroviral construct leading to irregular nuclear contours (Fischer et al. 1998).

The constitutive activation of different components of the MAPK (mitogen-activated protein kinase) pathway became apparent in PTC developing after radiation exposure as a result of *RET*, *NTRK1* (Rabes et al. 2000) or *B-RAF* gene rearrangements (Ciampi et al. 2005), but also in sporadic PTC harboring *B-RAF* point mutation (Nikiforova et al. 2003). The constitutive RET signaling in PTC1 and PTC3 tumors, whereby RAS-RAF-MAPK pathway is permanently activated (Fagin 2004; Fusco et al. 2005), influences certain cytoskeletal proteins as proven by our 2-DE studies, namely actin, cofilin-1 and vimentin.

An influence of continuous RET signaling on actin reorganization is corroborated by observations that in PC-PTC cells (rat thyroid epithelial cell line transfected with *RET/PTC1*) many thick actin bundles arranged in long stress fibers were detected, while parental cells had very few and short actin filaments (Barone et al. 2001). Fibroblasts (NIH3T3) and mammary epithelial cell lines (MCF7) microinjected with *RET/PTC1* do not form stress fibers, indicating that RET/PTC elicits a signaling pathway selectively active in thyroid cells (Barone et al. 2001). This observation could be confirmed, because the different actin species could not be detected in 2-DE gels of mouse NIH3T3 cells transfected and transformed by the human *RET/PTC1* oncogene (kindly provided by M.A. Pierotti; our unpublished results).

RAS acts as a central regulator of the cofilin dephosphorylation pathway. The cooperation of two RAS-initiated signaling pathways is required to induce cofilin activation by dephosphorylation, a RAS-RAF-MEK and a RAS-PI3K effector cascade (Nebl et al. 2004). Cofilin-1 dephosphorylation is finally induced by serine-phosphatase 1 and A2 (Samstag et al. 1996). It was reported that constitutively active phosphatases are involved in signal transduction due to the presence/activity of rearranged *RET* oncogene (Sakai et al. 1989). In addition, cofilin was detected to be induced in NIH3T3 cell lines expressing RET-MEN2A or RET-MEN2B, suggesting that an increase of cofilin contributes to the malignant properties of RET mutant protein-synthesizing cells (Watanabe et al. 2002).

Components of the MAPK pathway may also interact with vimentin, an indirect target of RAF-1, indicating that RAF-1 is linked to changes of the cytoskeletal architecture (Janosch et al. 2000). By immunohistochemical investigations, no detectable differences in vimentin amount between PTC with and without RET rearrangement could be detected (Soares et al. 1998; Vasko et al. 2007). However, discrimination of different protein species is not possible by immunohistochemistry. The enhanced amount of the different vimentin species observed in PTC1 and PTC3 tumors but not in PTC0 tumors reflects, therefore, the influence of constitutively active RET signaling.

In conclusion, our observation that distinct protein species of different cytoskeletal proteins, namely actin, vimentin as well as the actin-binding protein cofilin-1 were found to be significantly enhanced in PTC1 and PTC3 tumors and partially in lymph node metastases suggests that these modified protein amounts are induced by the activation of a single truncated rearranged gene. This reflects the importance to elucidate disease-related typical signatures on the protein species level.

Acknowledgments We are grateful to Sigrid Madsen-Unverfärth for skillful technical assistance in 2-DE and immunoblotting. This work was supported by a grant (to H.M.R.) from Deutsche Krebshilfe, Bonn, Germany.

References

Airaksinen MS, Titievsky A, Saarma M (1999) GDNF family neurotrophic factor signaling: four masters, one servant? Mol Cell Neurosci 13:313–325

Andreoli JM, Trevor KT (1994) Fate of a headless vimentin protein in stable cell cultures: soluble and cytoskeletal forms. Exp Cell Res 214:177–188

Barone MV, Sepe L, Melillo RM, Mineo A et al (2001) RET/PTC1 oncogene signaling in PC Cl 3 thyroid cells requires the small GTP-binding protein Rho. Oncogene 2:6973–6982

Basolo F, Pollina L, Fontanini G, Fiore L et al (1997) Apoptosis and proliferation in thyroid carcinoma: correlation with bcl-2 and p53 protein expression. Br J Cancer 75:537–541

Bongarzone I, Butti MG, Coronelli S, Borrello MG et al (1994) Frequent activation of ret protooncogene by fusion with a new activating gene in papillary thyroid carcinomas. Cancer Res 54:2979–2985

Brockstedt E, Rickers A, Kostka S, Laubersheimer A et al (1998) Identification of apoptosis-associated proteins in a human Burkitt lymphoma cell line. Cleavage of heterogeneous nuclear ribonucleoprotein A1 by caspase 3. J Biol Chem 273:28057–28064

Byun Y, Chen F, Chang R, Trivedi M et al (2001) Caspase cleavage of vimentin disrupts intermediate filaments and promotes apoptosis. Cell Death Differ 8:443–450

Carlier MF, Ressad F, Pantaloni D (1999) Control of actin dynamics in cell motility. Role of ADF/cofilin. J Biol Chem 274:33827–33830

Celetti A, Cerrato A, Merolla F, Vitagliano D et al (2004) H4(D10S170), a gene frequently rearranged with RET in papillary thyroid carcinomas: functional characterization. Oncogene 23:109–121

Ciampi R, Knauf JA, Kerler R, Gandhi M et al (2005) Oncogenic *AKAP9-BRAF* fusion is a novel mechanism of MAPK pathway activation in thyroid cancer. J Clin Invest 115:94–101

Fagin JA (2004) Challenging dogma in thyroid cancer molecular genetics—role of RET/PTC and BRAF in tumor initiation. J Clin Endocrinol Metab 89:4264–4266

Fischer AH, Bond JA, Taysavang P, Battles OE, Wynford-Thomas D (1998) Papillary thyroid carcinoma oncogene (RET/PTC) alters the nuclear envelope and chromatin structure. Am J Pathol 153:1443–1450

Fujita J, Bandoh S, Yang Y, Wu F et al (2003) High molecular weight vimentin complex is formed after proteolytic digestion of vimentin by caspase-3: detection by sera of patients with interstitial pneumonia. Microbiol Immunol 47:447–451

Fusco A, Chiappetta G, Hui P, Garcia-Rosta G et al (2002) Assessment of RET/PTC oncogene activation and clonality in thyroid nodules with incomplete morphological evidence of papillary carcinoma: a search for the early precursors of papillary cancer. Am J Pathol 160:2157–2167

Fusco A, Viglietto G, Santoro M (2005) A new mechanism of BRAF activation in human thyroid papillary carcinomas. J Clin Invest 115:20–23

Greco M, Santoro M, Berlingieri MT, Melillo RM et al (1999) PTC is a novel rearranged form of the ret proto-oncogene and is frequently detected in vivo in human thyroid papillary carcinomas. Cell 60:557–563

Hashimoto M, Inoue S, Ogawa S, Conrad C et al (1998) Rapid fragmentation of vimentin in human skin fibroblasts exposed to tamoxifen: a possible involvement of caspase-3. Biochem Biophys Res Commun 247:401–406

Janosch P, Kieser A, Eulitz M, Lovric J et al (2000) The Raf-1 kinase associates with vimentin kinases and regulates the structure of vimentin filaments. FASEB J 14:2008–2021

Jungblut PR, Seifert R (1990) Analysis by high-resolution two-dimensional electrophoresis of differentiation-dependent alterations in cytosolic protein pattern of HL-60 leukemic cells. J Biochem Biophys Methods 21:47–58

Khaitlina SY, Strzelecka-Golaszewska H (2002) Role of the DNase-I-binding loop in dynamic properties of actin filament. Biophys J 82:321–333

Kiessling P, Jahn W, Maier G, Polzar B, Mannherz HG (1995) Purification and characterization of subtilisin cleaved actin lacking the segment of residues 43–47 in the DNase I binding loop. Biochemistry 34:14834–14842

Klose J (1999) Fractionated extraction of total tissue proteins from mouse and human for 2-D electrophoresis. Methods Mol Biol 112:67–85

Klose J, Kobalz U (1995) Two-dimensional electrophoresis of proteins: an updated protocol and implications for a functional analysis of the genome. Electrophoresis 16:1034–1059

Klugbauer S, Lengfelder E, Demidchik EP, Rabes HM (1995) High prevalence of RET rearrangement in thyroid tumors of children from Belarus after the Chernobyl reactor accident. Oncogene 11:2459–2467

Lamer S, Jungblut PR (2001) Matrix-assisted laser desorption-ionization mass spectrometry peptide mass fingerprinting for proteome analysis: identification efficiency after on-blot or in-gel digestion with and without desalting procedures. J Chromatogr B Biomed Sci Appl 752:311–322

Lee SY, Song EJ, Kim HJ, Kang HJ et al (2001) Rac1 regulates heat shock responses by reorganization of vimentin filaments: identification using MALDI-TOF MS. Cell Death Differ 8:1093–1102

Mai KT, Landry DC, Thomas J, Yazdi et al (2001) Ret oncogene protein expression in papillary thyroid carcinoma and related lesions. Tumori 87:166–172

Mashima T, Naito M, Tsuruo T (1999) Caspase-mediated cleavage of cytoskeletal actin plays a positive role in the process of morphological apoptosis. Oncogene 18:2423–2430

Morishima N (1999) Changes in nuclear morphology during apoptosis correlate with vimentin cleavage by different caspases located either upstream or downstream of Bcl-2 action. Genes Cells 4:401–414

Muhlrad A, Kudryashov D, Michael Peyser Y, Bobkov AA et al (2004) Cofilin induced conformational changes in F-actin expose subdomain 2 to proteolysis. J Mol Biol 342:1559–1567

Nebl G, Fischer S, Penzel R, Samstag Y (2004) Dephosphorylation of cofilin is regulated through Ras and requires the combined activities of the Ras-effectors MEK and PI3K. Cell Signal 16:235–243

Nikiforov YE, Rowland JM, Bove KE, Monforte-Munoz H, Fagin JA (1997) Distinct pattern of ret oncogene rearrangements in morphological variants of radiation-induced and sporadic thyroid papillary carcinomas in children. Cancer Res 57:1690–1694

Nikiforova MN, Kimura ET, Gandhi M, Biddinger PW et al (2003) BRAF mutations in thyroid tumors are restricted to papillary carcinomas and anaplastic or poorly differentiated carcinomas arising from papillary carcinomas. J Clin Endocrinol Metab 88:5399–5404

Nylund R, Leszczynski D (2004) Proteomics analysis of human endothelial cell line EA.hy926 after exposure to GSM 900 radiation. Proteomics 4:1359–1365

Pierotti MA, Santoro M, Jenkins RB, Sozzi G et al (1992) Characterization of an inversion on the long arm of chromosome 10 juxtaposing D10S170 and RET and creating the oncogenic sequence RET/PTC. Proc Nat Acad Sci USA 89:1616–1620

Rabes HM (2001) Gene rearrangements in radiation-induced thyroid carcinogenesis. Med Pediatr Oncol 36:574–582

Rabes HM, Demidchik EP, Sidorow JD, Lengfelder E et al (2000) Pattern of radiation-induced RET and NTRK1 rearrangements in 191 post-Chernobyl papillary thyroid carcinomas: biological, phenotypic, and clinical implications. Clin Cancer Res 6:1093–1103

Sakai R, Ikeda I, Kitani H, Fujiki H et al (1989) Flat reversion by okadaic acid of raf and ret-II transformants. Proc Natl Acad Sci USA 86:9946–9950

Samstag Y, Dreizler EM, Ambach A, Sczakiel G, Meuer SC (1996) Inhibition of constitutive serine phosphatase activity in T lymphoma cells results in phosphorylation of pp19/cofilin and induces apoptosis. J Immunol 156:4167–4173

Santoro M, Dathan NA, Berlingieri MT, Bongarzone I et al (1994) Molecular characterization of RET/PTC3: a novel rearranged version of the RET proto-oncogene in a human thyroid papillary carcinoma. Oncogene 9:509–516

Sariola H, Saarma M (2003) Novel functions and signalling pathways for GDNF. J Cell Sci 116:3855–3862

Sarria AJ, Lieber JG, Nordeen SK, Evans RM (1994) The presence or absence of a vimentin-type intermediate filament network affects the shape of the nucleus in human SW-13 cells. J Cell Sci 107:1593–1607

Shoeman RL, Hartig R, Traub P (1999) Characterization of the nucleic acid binding region of the intermediate filament protein vimentin by fluorescence polarization. Biochemistry 38:16802–16809

Shoeman RL, Huttermann C, Hartig R, Traub P (2001) Amino-terminal polypeptides of vimentin are responsible for the changes in nuclear architecture associated with human immunodeficiency virus type 1 protease activity in tissue culture cells. Mol Biol Cell 12:143–154

Soares P, Fonseca E, Wynford-Thomas D, Sobrinho-Simões M (1998) Sporadic RET-rearranged papillary carcinoma of the thyroid: a subset of slow growing, less aggressive thyroid neoplasms? J Pathol 185:71–78

Thomas GA, Bunnell H, Cook HA, Williams ED et al (1999) High prevalence of RET/PTC rearrangements in Ukrainian and Belarussian post-Chernobyl thyroid papillary carcinomas: a strong correlation between RET/PTC3 and the solid-follicular variant. J Clin Endocrinol Metab 84:4232–4238

Vasko V, Espinosa AV, Scouten W, He H et al (2007) Gene expression and functional evidence of epithelial-to-mesenchymal transition in papillary thyroid carcinoma invasion. Proc Natl Acad Sci USA 104:2803–2808

Wang Q, Shoeman R, Traub P (2000) Identification of the amino acid residues of the amino terminus of vimentin responsible for DNA binding by enzymatic and chemical sequencing and analysis by MALDI-TOF. Biochemistry 39:6645–6651

Watanabe T, Ichihara M, Hashimoto M, Shimono K et al (2002) Characterization of gene expression induced by RET with MEN2A or MEN2B mutation. Am J Pathol 161:249–256

Yeh S, Chang C (1996) Cloning and characterization of a specific coactivator ARA70 for the androgen receptor in human prostate cells. Proc Natl Acad Sci USA 93:5517–5521

Zeindl-Eberhart E, Rabes HM (1992) Variant protein patterns in hepatomas and transformed liver cell lines as determined by high resolution two-dimensional gel electrophoresis (2DE). Carcinogenesis 13:1177–1183

Zeindl-Eberhart E, Jungblut PR, Rabes HM (1997) A new method to assign immunodetected spots in the complex two-dimensional electrophoresis pattern. Electrophoresis 18:799–801

Zeindl-Eberhart E, Klugbauer S, Dimitrijevic N, Jungblut PR et al (2001) Proteome analysis of rat hepatomas: carcinogen-dependent tumor-associated protein variants. Electrophoresis 22:3009–3018